

# Targeted Treatment of Metastatic Breast Cancer by PLK1 siRNA Delivered by an Antioxidant Nanoparticle Platform

Jingga Morry<sup>1</sup>, Worapol Ngamcherdtrakul<sup>1,2</sup>, Shenda Gu<sup>1</sup>, Moataz Reda<sup>1</sup>, David J. Castro<sup>1,2</sup>, Thanapon Sangvanich<sup>1</sup>, Joe W. Gray<sup>1</sup>, and Wassana Yantasee<sup>1,2</sup>

## Abstract

Metastatic breast cancer is developed in about 20% to 30% of newly diagnosed patients with early-stage breast cancer despite treatments. Herein, we report a novel nanoparticle platform with intrinsic antimetastatic properties for the targeted delivery of Polo-like kinase 1 siRNA (siPLK1). We first evaluated it in a triple-negative breast cancer (TNBC) model, which shows high metastatic potential. PLK1 was identified as the top therapeutic target for TNBC cells and tumor-initiating cells in a kinome-wide screen. The platform consists of a 50-nm mesoporous silica nanoparticle (MSNP) core coated layer-by-layer with bioreducible cross-linked PEI and PEG polymers, conjugated with an antibody for selective uptake into cancer cells. siRNA is loaded last and fully protected under the PEG layer from blood enzymatic degradation. The material has net neutral charge and

low nonspecific cytotoxicity. We have also shown for the first time that the MSNP itself inhibited cancer migration and invasion in TNBC cells owing to its ROS- and NOX4-modulating properties. *In vivo*, siPLK1 nanoconstructs (six doses of 0.5 mg/kg) knocked down about 80% of human *PLK1* mRNA expression in metastatic breast cancer cells residing in mouse lungs and reduced tumor incidence and burden in lungs and other organs of an experimental metastasis mouse model. Long-term treatment significantly delayed the onset of death in mice and improved the overall survival. The platform capable of simultaneously inhibiting the proliferative and metastatic hallmarks of cancer progression is unique and has great therapeutic potential to also target other metastatic cancers beyond TNBC. *Mol Cancer Ther*; 16(4); 763–72. ©2017 AACR.

## Introduction

About 1.7 million new cases of breast cancer were diagnosed worldwide in 2012 (1), and around 250,000 more are expected to be diagnosed in the United States in 2016 (2). About 20% to 30% of newly diagnosed patients with early-stage breast cancer will develop distant metastasis despite the treatments. There is no effective distant treatment for metastatic cancer so far, current treatment focuses on slowing disease progression and maintaining the quality of life. Targeted delivery of siRNAs by nanoparticles holds great promise for cancer treatment, as siRNA can target any gene deemed important to cancer progression, metastasis, and drug resistance with high specificity (3). To that end, we have recently developed and optimized a polymer-coated mesoporous silica nanoparticles (MSNP) for siRNA delivery to treat trastuzumab-resistant HER2<sup>+</sup> breast tumors (4). The platform consists of a

50-nm MSNP core coated layer-by-layer with bioreducible cross-linked 10-kDa polyethyleneimine (PEI) for effective siRNA binding and endosomal escape and polyethylene glycol (PEG) for preventing nanoparticle aggregation, minimizing enzyme degradation of siRNAs, shielding the toxic effect of PEI, and reducing recognition by the immune system. In addition, a targeting antibody can be attached to the PEG layer to serve as a homing agent on the nanoparticle. The siRNA is then loaded last onto the nanoparticle, passing the PEG layer (due to small size) and binding to the PEI layer due to charge preference (See Supplementary Fig. S1).

Herein, we report for the first time that the same platform can act as a targeted siRNA delivery system to metastatic breast tumors. For the siRNA target, we chose polo-like kinase 1 (PLK1), which is involved in cell division and DNA damage response and is found in actively dividing cancer cells (5). PLK1 was identified as a promising therapeutic target for cancer treatment (6). There is strong association between elevated PLK1 levels in breast tumors and poor clinical outcome (7). Moreover, a recent genome-wide kinase screen also identified PLK1 as the strongest kinase target as demonstrated by significant cell death in both cancer and tumor-initiating cells (TIC) in triple-negative breast cancer (TNBC) when either knocked down or inhibited (8). PLK1 inhibitor, BI2536, had reached clinical trials but was terminated because of poor therapeutic index, as the systemic delivery of PLK1 inhibitors was associated with increased incidence neutropenia and thrombocytopenia (9). In addition, PLK1 inhibitors (e.g., BI2536, BI6727, GSK461364) can also inhibit other PLK family members PLK2 and PLK3, which may lead to unwanted off-target effects (10). In

<sup>1</sup>Department of Biomedical Engineering, Oregon Health and Science University, Portland, Oregon. <sup>2</sup>PDX Pharmaceuticals, LLC, Portland, Oregon.

**Note:** Supplementary data for this article are available at Molecular Cancer Therapeutics Online (<http://mct.aacrjournals.org/>).

J. Morry and W. Ngamcherdtrakul contributed equally to this study.

**Corresponding Authors:** Joe W. Gray, 2730 SW Moody Ave, CL3G, Portland, OR 97201. Phone: 503-494-6500; Fax: 503-418-9311; E-mail: grayjo@ohsu.edu; and Wassana Yantasee, 3303 SW Bond Ave, CH13B, Portland, OR 97239. Phone: 503-418-9306; Fax: 503-418-9311; E-mail: yantasee@ohsu.edu

**doi:** 10.1158/1535-7163.MCT-16-0644

©2017 American Association for Cancer Research.

Morry et al.

contrast, siRNA can be designed to target only PLK1 and thus have less toxicity to non-cancer cells than BI2536 (11). An siRNA against PLK1 (TKM-080301) has been in phase I/II trials by Arbutus Biopharma, but the delivery platform has no targeting agent and is lipid-based that is homing for liver. When used to treat liver tumors, stable disease in 51% of 43 patients was reported (12) but with a narrow therapeutic window due to toxicity (0.6–0.75 mg/kg; ref. 13). We hypothesize that siRNA sequence specificity and the delivery specificity will improve both efficacy and safety.

Another unique and important feature about our platform is the inherent antioxidant activity of the mesoporous silica core. This antioxidant capability is shown herein to have pronounced effects in inhibiting epithelial-to-mesenchymal transition (EMT) and cellular invasion *in vitro*. ROS plays an important role in cancer metastasis (14). ROS-generating NOX4 is crucial in redox-mediated signaling pathways, including Tks5-dependent invadopodia formation (15), TGF- $\beta$ /SMAD3-driven EMT and cell migration (16), and PI3K/Akt-regulated cell proliferation and invasion (17). Reduction of ROS using an antioxidant, such as *N*-acetylcysteine (NAC), or the NOX inhibitor, diphenyleneiodonium (DPI), successfully decreased cancer invasion and invadopodia formation (15). Nevertheless, these agents are not used in clinics for such purposes due to the inability to achieve sufficient cellular NAC levels based on the current prescribed dose (18) and the challenge of getting specificity to particular NOX isoforms (19). Thus, a material that can scavenge ROS at cellular levels can offer an effective therapy for metastatic breast cancer. Of the 162 investigational new drugs (IND) in clinical trials for treating metastatic breast cancer, only one targets the cancers' ability to activate invasion and metastasis (a TGF- $\beta$  inhibitor) and most target cancers' sustaining proliferative signaling (20). Our material is uniquely targeting both cancer hallmarks, making it highly novel.

## Materials and Methods

### Synthesis and characterization of nanoparticles and siRNA loading

MSNPs of 50 nm in size were synthesized and surface-modified as in our previous report (4). MSNP cores were measured for primary (dry) size by a Transmission Electron Microscope (Philips/FEI Tecnai TEM). After chemical modifications, the material was measured for hydrodynamic size in PBS (pH 7.2) with a Zetasizer (Malvern). PEI and PEG loadings were quantified by a thermogravimetric analyzer (TGA Q50, TA Instruments). siRNA loading was accomplished with 10-minute mixing in PBS. The siRNA loading was quantified by fluorescence detection of dye-tagged siRNA as well as gel electrophoresis. The material contained 14 wt% 10-kDa PEI, 18 wt% 5-kDa PEG, 3 wt% antibody or no antibody, and 2 wt% siRNA. It is referred to as T-siRNA-NP with trastuzumab (T) antibody or siRNA-NP without (4). The particle size in PBS was  $104 \pm 1.7$  nm and the charge decreased from  $13.3 \pm 0.70$  mV to  $8.10 \pm 0.25$  mV once loaded with siRNA (measured in 10 mmol/L NaCl), which falls within neutral range as defined by Nanotechnology Characterization laboratory of NCI (21). Schematic illustration of the nanoconstruct can be found in Supplementary Fig. S1.

### Cell culture and transfection

Human breast carcinoma cell lines, BT549 and MDA-MB-231, were obtained from ATCC and maintained in RPMI with 10% FBS. LM2-4luc<sup>+</sup>/H2N (22) was a gift from Prof. Robert Kerbel

(University of Toronto, Toronto, ON, Canada) and Prof. Giulio Francia (now at University of Texas at El Paso, El Paso, TX) and maintained in RPMI + 5% FBS. BT549 and MDA-MB-231 were authenticated by genotyping at the Sequencing Core of Oregon Health and Science University (OHSU; Portland, OR) and both matched genotypes available from ATCC. LM2-4luc<sup>+</sup>/H2N, a derived cell line as described in ref. 22, was used as received and not authenticated in our laboratory. For nanoparticle transfection (loaded with siSCR or siPLK1), cells (3,000 cells per well in 96-well plates or 200,000 cells in 6-well plates) were seeded overnight in complete medium and transfected with nanoparticle for 24 hours. The cells were washed once with PBS on the next day and incubated in a fresh cell media for 24 to 72 hours posttreatment depending on the type of the assays. Positive controls were carried out using DharmaFECT-1 transfection reagent (GE Dharmacon) diluted in OptiMEM medium (ThermoFisher Scientific). Unless stated otherwise, all experiments were performed with nanoparticle-to-siRNA mass ratio of 50 and 50 nmol/L siRNA throughout the study.

### siRNAs

Four different PLK1 siRNA sequences were purchased from Qiagen (cat. #1027416) for siRNA screening in the LM2-4luc<sup>+</sup>/H2N cell line. The *in vivo* grade siRNA was custom made by GE Dharmacon based on the sequence identified to yield the highest PLK1 gene knockdown and cell death in LM2-4luc<sup>+</sup>/H2N cells (see Supplementary Fig. S2). The siRNA sequences were as follows: optimal PLK1 (antisense 5'-UAUUCAUUCUUCUU-GAUCCGG-3'); scrambled SCR (antisense 5'-UUAUGCGACAU-GUAAACCA-3'). DY677-siSCR was custom made with DyLight 677 attached to the sense strand of the siSCR (GE Dharmacon).

### Animal studies

The experimental protocol was approved by the Institutional Animal Care and Use Committee (IACUC) of OHSU. Six- to 8-week old SCID hairless SHO (CrL:SHO-Prkdc<sup>scid</sup>Hr<sup>hr</sup>, Charles River) mice received intravenous tail vein injections of  $2 \times 10^6$  LM2-4luc<sup>+</sup>/H2N cells (suspended in 200  $\mu$ L PBS) and were allowed to establish metastasis in lungs for 2 weeks before initiating the treatments. For both studies (short-term and long-term), all mice were randomly divided into 3 treatment groups ( $n = 8$ /group): saline control, T-siSCR-NP (0.5 mg/kg siSCR), and T-siPLK1-NP (0.5 mg/kg siPLK1), with a dosing schedule of twice weekly by intravenous injection (Fig. 4A). IVIS imaging was done once weekly starting from 1 week postinoculation, following the protocol established by Caliper Life Sciences. Briefly, each animal received intraperitoneal injection of 150 mg/kg of D-luciferin (Gold Bio Technology, Inc.) in 200  $\mu$ L PBS, 10 minutes before imaging with IVIS spectrum Imaging system on prone and supine positions. The average photon flux (of prone and supine positions) for each mouse was quantified within the same area of interest in the thoracic region of each mouse. The flux was plotted as average fold change (relative to the pretreatment signals of each mouse) as a function of time. Body weight was measured twice weekly. For the short-term *in vivo* study, all animals were sacrificed 2 days after receiving the sixth dose of treatment, and their major organs (brain, heart, lung, liver, spleen, kidney, lymph nodes, and spine) were harvested and immersed in 300  $\mu$ g/mL of D-luciferin (in PBS) in a 24-well plate for 5 minutes before *ex vivo* IVIS imaging and signal quantification. Organs with detectable IVIS signals compared with negative

controls (i.e., the same organs from mice without tumor inoculation) were considered positive for the presence of cancer and included in "incidence rate." The tumor burden was calculated as the sum of all signals from each respective tumor-bearing organ.

For the long-term *in vivo* study, animals (8 animals per group) received the same dose and treatment schedule as the short-term study but the study was extended to 2 months. Mice were monitored daily for signs of illness (hind limb paralysis from suspected spine metastasis), excessive weight loss (>10% body weight loss compared with the preinoculation weight), visible tumors (from lymph nodes, with size > 1,500 mm<sup>3</sup>), or labored breathing from lung metastasis and were euthanized in accordance with IACUC ethical guidelines. All major organs were collected, weighed, and fixed for histologic analyses.

### Lung metastasis quantification

The lung tissues from each mouse were collected and fixed in 4% paraformaldehyde and snap-frozen in optimal cutting temperature (OCT) compound (#4583, Tissue-Tek) before processing. Tissue sections (6- $\mu$ m thick) were stained with hematoxylin and eosin (H&E). To assess the metastatic area, 10 sections of the entire lung at 160  $\mu$ m apart were scanned using ScanScope XT Digital Slide Scanner (Aperio), and the area of each metastatic lesion was measured relative to the total lung area.

For determination of the tumor burden and human *PLK1* mRNA expression in mouse lungs, lung tissue from each mouse was homogenized and lysed in RLT buffer using QIA-shredder columns (Qiagen), and the RNA was isolated using RNeasy Mini kit (Qiagen) following the manufacturer's protocol. RT-PCR (100 ng RNA per sample per reaction) was performed to identify the ratio of human *HPRT* mRNA (Hs99999909\_m1) relative to mouse *HPRT* mRNA (Mm03024075\_m1) for tumor burden or human *PLK1* mRNA (Hs00983225\_g1) relative to human *HPRT* mRNA to assess *PLK1* gene knockdown as a result of the treatments.

### Statistical analysis

*In vitro* experiments were performed in triplicates (experimentally and analytically), and the results were presented as mean  $\pm$  SD. *In vivo* experimental data were presented as mean  $\pm$  SEM. Comparisons of all groups at a single time point were performed after testing for D'Agostino–Pearson omnibus normality tests (GraphPad Prism 6.0). Comparisons of 2 groups were performed either with Student *t* tests (for normal distribution) or Mann–Whitney test (for nonparametric test, unpaired groups). For comparisons of more than 3 groups, statistical analysis was done either with one-way ANOVA with *post-hoc* Dunnett multiple comparison tests (for normal distribution) or Kruskal–Wallis nonparametric test with *post-hoc* Dunnett multiple comparison tests (for non-normal distribution). Two-way ANOVA followed by *post-hoc* Tukey multiple comparison tests was performed to analyze the treatment effects over time in the photon flux measurement of the *in vivo* study. Survival curves were analyzed using Kaplan–Meier and its multiple comparison tests were analyzed using log-rank test methods with adjusted alpha by Bonferroni correction. GraphPad Prism 6.0 software (GraphPad Software Inc.) was utilized for all statistical analyses. *P* < 0.05 was considered to be statistically significant.

Detailed procedures of intracellular ROS assay, cell viability assay, *in vitro* scratch assay, gelatin degradation, Matrigel invasion

assay, 3D culture, qPCR, Western blotting, and histology can be found in the Supplementary Methods.

## Results

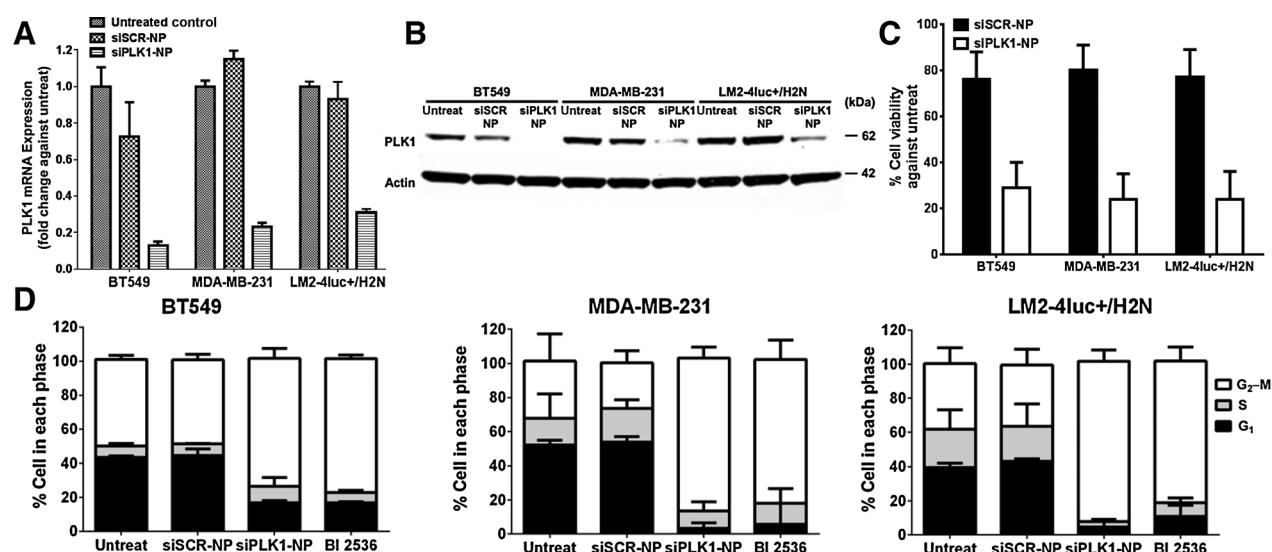
### *PLK1* knockdown efficacy and resultant apoptotic cell death

We chose TNBC cell lines for the *in vitro* studies due to their high metastatic potential. To investigate the silencing efficacy of siPLK1-NP *in vitro*, we treated BT549, MDA-MB-231, and LM2-4luc<sup>+</sup>/H2N (HER2-expressing MDA-MB-231 metastatic variant; ref. 22) cell lines with siPLK1-NP (without targeting agent) and measured the mRNA and protein expressions 24 and 48 hours posttreatment, respectively. As shown in Fig. 1A and B, siPLK1-NP efficiently reduced the *PLK1* mRNA by 69% to 87% and protein expressions by 64% to 91% in the 3 cell lines compared with the untreated control. Consequently, the siPLK1-NP treatment induced significant loss of cell viability measured at 3 days (Fig. 1C). We also confirmed that the siPLK1-NP treatment caused G<sub>2</sub>–M cell-cycle arrest at 24 hours posttreatment similar to the *PLK1* inhibitor BI-2536 (Fig. 1D). On the contrary, nontargeting siSCR-NP did not cause any significant reduction in the *PLK1* expression (Fig. 1A and B), was not toxic to the cells (~80% cell viability, Fig. 1C), and did not alter cell-cycle arrest compared with the untreated (Fig. 1D). These results demonstrate that the nanoparticle is well tolerated and can effectively deliver siPLK1 intracellularly, leading to apoptotic death of the TNBC cell lines.

### Antioxidant and NOX4 reduction properties of nanoparticle in TNBC cell lines

From our recent report (23), the MSNP core of our nanoparticle had ROS-scavenging and NOX4 reduction ability in TGF- $\beta$ -stimulated dermal fibroblast cells, yielding greater anti-fibrotic properties (e.g., reducing COL1 and  $\alpha$ -SMA) than observed with NAC treatment. Herein, we investigated the antioxidant effects of nanoparticle treatment on breast cancer cells. We included siSCR on the nanoparticle treatment to maintain similar size and charge of the nanoconstruct (and hence cellular uptake) as those of the siPLK1-NP. This siSCR does not have any significant sequence homology to known human or mouse genes. The ROS levels of all 3 TNBC cell lines were significantly higher (by 2- to 8-fold) than the nontumorigenic breast epithelial cells line, MCF10A (Supplementary Fig. S3A and S3B). Pretreatment of the breast cancer cell lines with siSCR-NP prior to ROS stimulation by menadione lowered the ROS levels by 60% to 84% compared with the menadione alone (Fig. 2A). The nanoparticle performed in a similar manner as the antioxidant NAC and NADPH oxidase (NOX) inhibitor DPI. Because NOX is a major source of ROS production, we measured the mRNA levels of NOX family members in the TNBC cell lines versus those in the nontumorigenic breast epithelial cell line, MCF10A. Of the 4 NOX family members tested, *NOX4* mRNA levels were significantly higher (than *NOX1*, *NOX3*, and *NOX5*) for all the TNBC cell lines compared with MCF10A (Supplementary Fig. S3C). In addition to its high level, *NOX4* (and ROS) has been shown to play very important roles in cancer invasion and metastasis via invadopodia formation (15), thus we further focused on *NOX4*. Treatment of siSCR-NP for 24 hours was able to significantly reduce *NOX4* mRNA in the TNBC cell lines by 37% to 56% compared with the untreated cells (Fig. 2B), similar to NAC and DPI. Interestingly, in terms of *NOX4* protein reduction, siSCR-NP lowered *NOX4* expression better than NAC and DPI after 72-hour treatment (Fig. 2C), suggesting

Morry et al.

**Figure 1.**

Effective knockdown of PLK1 with siPLK1-NP leads to G<sub>2</sub>-M cell-cycle arrest and reduced viability of 3 TNBC cell lines (BT549, MDA-MB-231, and LM2-4luc+/H2N). **A**, Expression levels of *PLK1* mRNA after treatment with either siSCR- or siPLK1-NP for 24 hours, as measured by qPCR, and normalization to GAPDH expression. **B**, Protein expression of PLK1 after 48 hours, as assessed by Western blotting with actin as the loading control. **C**, Cell viability after 72 hours. **D**, Cell-cycle analysis after 24-hour treatment with siSCR-, siPLK1-NP, or 10 nmol/L of BI2536. All with siRNA doses of 50 nmol/L. All data are presented as mean  $\pm$  SD from 3 independent experiments.

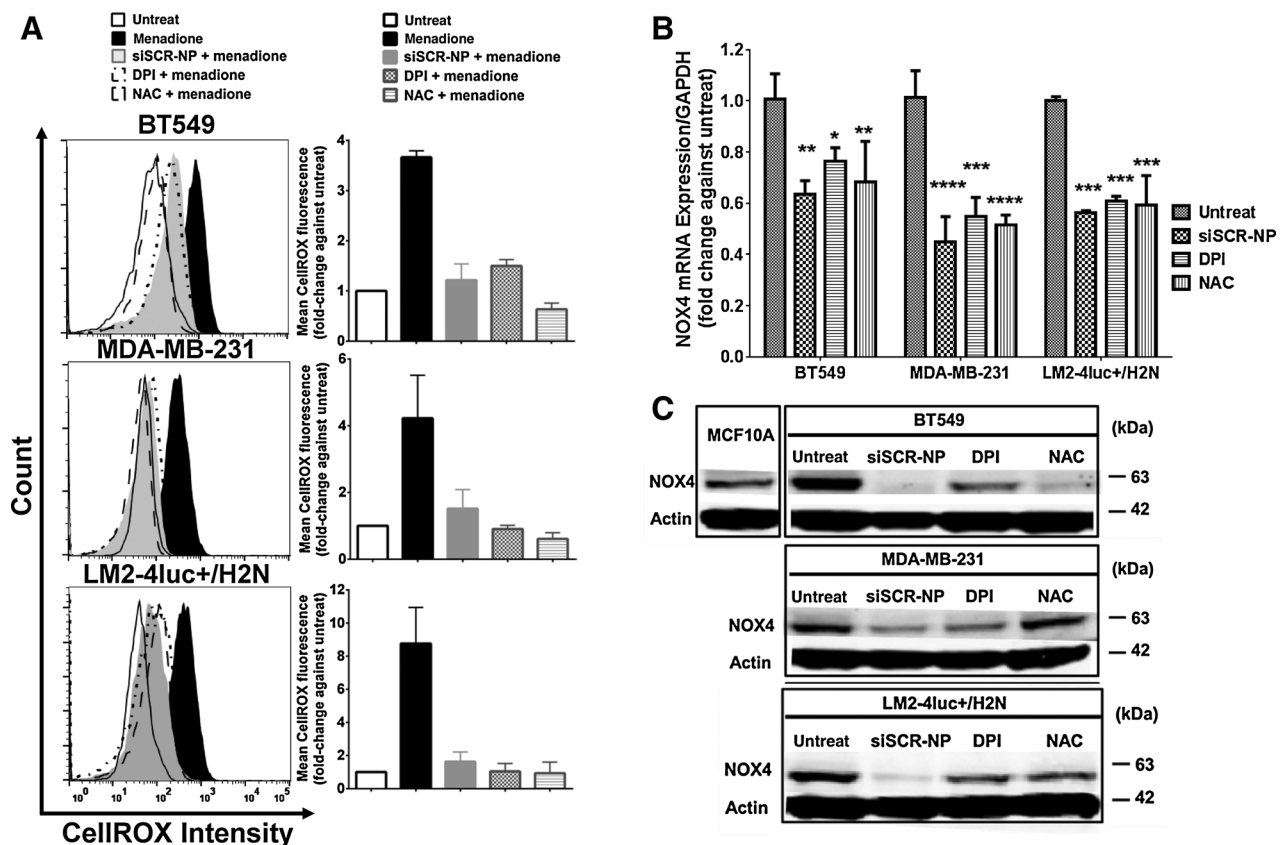
that nanoparticle may have more sustainable effect than NAC and DPI. Taken together, these results proved that nanoparticle, indeed, possessed ROS-scavenging ability. The ability of nanoparticle to reduce NOX4 expression upon ROS scavenging also indicates a positive feedback loop between ROS and NOX4. Interestingly, the nanoparticle did not significantly reduce the ROS level of the MCF10A (Supplementary Fig. S3D) likely due to the low baseline level of ROS and NOX4 in this cell line compared with the 3 TNBC cell lines (Supplementary Fig. S3A–S3C).

#### Nanoparticle treatment inhibits cellular migration and invasion and attenuates outgrowth of 3D organotypic cultures

Elevated levels of ROS have been known to promote cellular migration as well as invasion (24). To investigate the effects of nanoparticle treatment on cellular migration, we performed an *in vitro* scratch assay using the LM2-4luc<sup>+</sup>/H2N cell line. We used nanoparticle without trastuzumab (T) throughout the migration, invasion, and 3D growth studies to ensure that any observed effect was due to the nanoparticle itself and not trastuzumab. The cells were wounded (25) following a 24-hour pretreatment with siSCR- or siPLK1-NP. DharmaFECT commercial transfection reagent delivering both siRNAs was also used as controls. We monitored wound closure at 24 hours and reported it as the percentage of wound recovery relative to the wound size at  $t = 0$  hour. Figure 3A shows the representative wound recovery images, and Fig. 3B shows the quantification. Cells treated with siSCR-NP and siPLK1-NP displayed the least wound recovery indicating slowest cell migration compared with the untreated control and DharmaFECT counterparts. This was not due to the siSCR or siPLK1, as when delivered with DharmaFECT, they showed no inhibitory effect on cell migration. Moreover, we delivered nanoparticle loaded with

fluorescently labeled siRNA, DyLight 677 (DY677siSCR-NP) to ensure that the effect was attributed to the intracellular presence of NP and not a physical hindrance at the wound border (Fig. 3A).

Next, we investigated the ability of nanoparticle to migrate through the extracellular matrix (ECM) by forming the actin-rich protrusions known as invadopodia. Specifically, we cultured cells that were pretreated with siSCR-NP or DPI on thin fluorescent gel matrices for 24 hours and measured the area of gelatin degradation. Higher gelatin degradation indicates higher invadopodia formation which correlates to the cellular invasive potential. As shown in Fig. 3C and D, siSCR-NP treatment reduced gelatin degradation activity by about 42% compared with the untreated groups, indicating reduction of invadopodia formation by the nanoparticle. The effect is on par with DPI treatment (~46%). To confirm our finding, we also measured the invasive capacity of the cells in a Matrigel-coated Boyden chamber assay. Nanoparticle treatment markedly reduced the invasiveness of the cells by about 65%, in a similar manner as DPI (~60%), as compared with the untreated control (Fig. 3E). Only the high dose of NAC (30 mmol/L) produced inhibitory effects on the invasiveness of the cells in the same par with nanoparticle and DPI. This is in agreement with previous report demonstrating that only a high NAC dose (20–40 mmol/L) was able to reduce cancer cell invasion (15). Conversely, the observed increase in invaded cells at the low dose of NAC (2–5 mmol/L, Fig. 3E) is also in line with another observation (26), showing that low levels of NAC increased cancer metastasis potential *in vivo*. However, high levels of NAC are not achievable in blood (not even 10 mmol/L), based on the current prescribed dose of NAC (18). Thus, our antioxidant nanoparticle has a clear advantage over NAC. Specifically, much less dose of nanoparticle required to achieve the same effect as NAC may be attributed to extremely large scavenging sites (from large surface area of the MSNP, ~500 m<sup>2</sup>/g).

**Figure 2.**

Nanoparticle shows antioxidant activity and NOX4 reduction in 3 TNBC cell lines (BT549, MDA-MB-231, and LM2-4luc<sup>+</sup>/H2N). **A**, ROS levels of the cells after 24-hour treatment with siSCR-NP (50 nmol/L), DPI (5  $\mu$ mol/L), or NAC (20 mmol/L), followed by 1-hour treatment with 100  $\mu$ mol/L of menadione, assessed by CellROX flow cytometry. Expression levels of **(B)** NOX4 mRNA at 24 hours and **(C)** NOX4 protein at 72 hours of the 3 cell lines after receiving similar treatments with **(A)** for 24 hours but without menadione. All mRNA data were measured by qPCR and normalized to GAPDH expression. Data are presented as mean  $\pm$  SD from 3 independent experiments. \*,  $P < 0.05$ ; \*\*,  $P < 0.01$ ; \*\*\*,  $P < 0.001$ ; \*\*\*\*,  $P < 0.0001$  versus untreated.

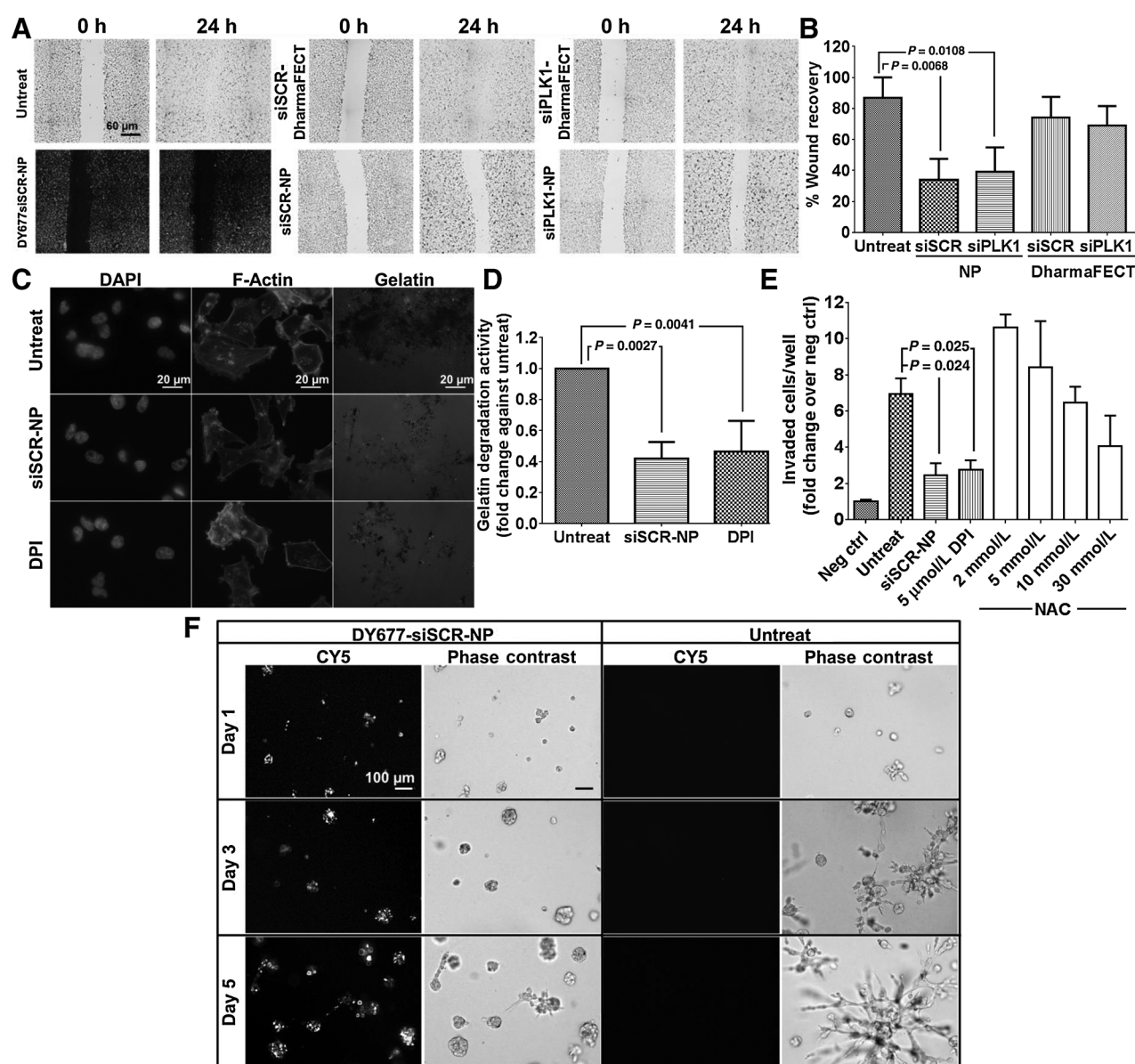
To study the effects of nanoparticle treatment in a 3D environment, we seeded cells (pretreated with DY677siSCR-NP) on Matrigel-coated plates and observed the cell phenotypes from day 1 to 5 post-seeding. LM2-4luc<sup>+</sup>/H2N cells grown in 3D culture exhibited stellate structures (Fig. 3F), which is typical for highly invasive cells such as its parental MDA-MB-231 cell line (27). However, treatment with siSCR-NP inhibited the invasive growth patterns of these cells, resulting in more rounded spheroid structures. To ensure that nanoparticle was still present within the cells, we also imaged the cells in the fluorescence channel (for viewing DY677siSCR-NP) up to 5 days post-seeding on Matrigel (Fig. 3F). These experiments demonstrate that nanoparticle treatment effectively reduced cellular migration and invasiveness of a highly invasive breast cancer cell line *in vitro*.

#### Ability of T-NP to deliver siRNAs and elicit therapeutic effects in a mouse model of metastasis

A breast cancer metastasis model was established upon tail vein injection of LM2-4luc<sup>+</sup>/H2N cells (from Dr. Robert Kerbel's laboratory, University of Toronto), a highly metastatic variant of MDA-MB-231 (TNBC) which was isolated from lung metastasis in

mice (28) and has been shown to develop metastasis in multiple organs (29). This cell line was later engineered to express luciferase and *HER2* genes (22). We found siPLK1 to be highly effective in killing this cell line (see Fig. 1). Despite overexpressing *HER2*, we found that this cell line behaved like its parental MDA-MB-231 cell in that it did not respond to trastuzumab (0–30  $\mu$ g/mL) as a free drug or when conjugated to the NP (T-NP) *in vitro* (Supplementary Fig. S4). Nevertheless, the *HER2* protein can serve as the homing target receptor to facilitate targeted delivery of siPLK1 utilizing the nanoparticle conjugated with trastuzumab (T-NP). The cellular uptake specificity of T-NP to *HER2*<sup>+</sup> cells over *HER2*<sup>-</sup> cells has been previously reported (4). In mice, tumors were allowed to establish for 2 weeks until luciferase signals were detected in lungs by IVIS (Fig. 4B), followed by twice weekly tail vein injections of T-siPLK1-NP for both the short- and long-term studies. Dosing and schedule are shown in Fig. 4A (frequency optimization as described in Supplementary Methods). After a total of 6 doses treatment (0.5 mg/kg siRNA per injection per mouse), T-siPLK1-NP exhibited significantly reduced tumor burden in the lungs compared with the saline and T-siSCR-NP groups (Fig. 4C). This was also reflected in the constant body weight of the animals treated with T-siPLK1-NP, whereas those treated with

Morry et al.

**Figure 3.**

Nanoparticle treatment impedes cellular migration and reduces cellular invasiveness of LM2-4luc<sup>+</sup>/H2N cell line. **A**, Representative images of *in vitro* scratch assay with siSCR or siPLK1 on nanoparticle or on DharmaFECT (all with 50 nmol/L as siRNA). Cells were treated for 24 hours prior to wound scratch and images were taken at 0 and 24 hours post-scratch. **B**, Percentage of wound recovery area from (A) using ImageJ. Data are presented as mean  $\pm$  SD from 3 independent experiments ( $n = 8-10$  images/well, duplicate wells per experiment). **C**, Representative images from gelatin degradation assay. Cells were pretreated with 50 nmol/L siSCR-NP or 5  $\mu$ mol/L DPI before seeding on the FITC-gelatin-coated coverslips for 24 hours. Cells were stained for F-actin and nuclei. **D**, Percentage of gelatin degradation per total number of cells in (C) by ImageJ. Data are presented as mean  $\pm$  SD from 3 independent experiments ( $n = 5$  images/well, >50 cells/field, duplicate wells per experiment). **E**, Invasion of LM2-4luc<sup>+</sup>/H2N cells after 48-hour treatment with 50 nmol/L siSCR-NP, 5  $\mu$ mol/L DPI, or 2 to 30 mmol/L NAC through Matrigel-coated Boyden chambers, normalized by negative controls (number of cells invaded through chambers with no serum added). Data are represented as mean  $\pm$  SD from 2 independent experiments performed in duplicates. **F**, Representative images of LM2-4luc<sup>+</sup>/H2N cells pretreated with 50 nmol/L DY677siSCR-NP before seeding in 3D Matrigel culture versus untreated and imaged on days 1, 3, and 5 post-seeding.

saline and T-siSCR-NP experienced weight loss likely due to advanced cancer metastases (Fig. 4D). At 2 days after the last dose, the study was concluded, and the organs from each mouse were imaged *ex vivo* with IVIS (Supplementary Fig. S5C). Tumor incidence rates (organs with positive IVIS signals relative to the

respective organs of normal mice) as well as tumor burden (photon flux relative to the respective organs of normal mice) are presented in Table 1. Tumors were detected in fewer organs with the T-siSCR-NP treatment (vs. untreated) and in fewest organs with T-siPLK1-NP treatment (Table 1). H&E-stained and

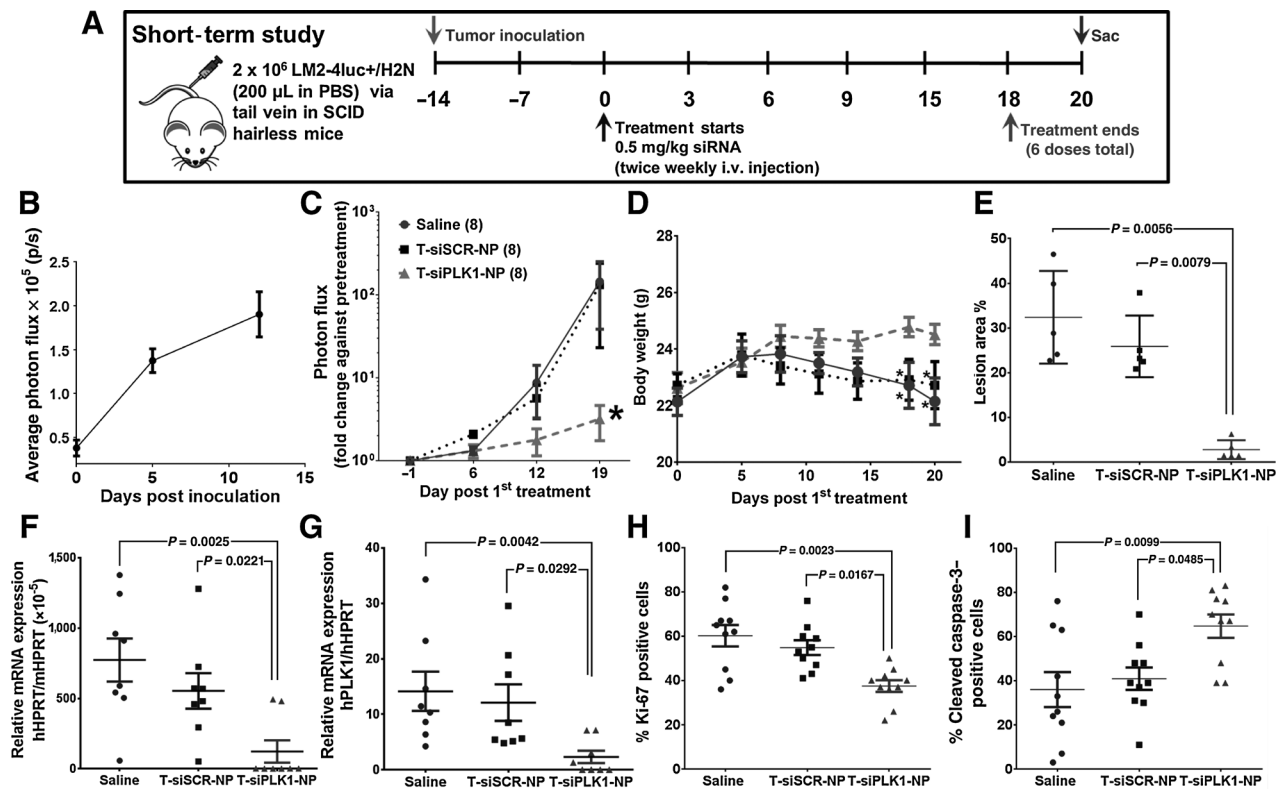


**Figure 4.**

Effects of T-siPLK1-NP treatment in the *in vivo* experimental metastasis model. **A**, Schematic representation of the study design for the short-term *in vivo* study. **B**, Quantification of lung photon flux (by weekly IVIS) showing cancer being established in lungs post inoculation. **C**, Lung photon flux normalized to pretreatment flux from each individual mouse in the same treatment groups. **D**, Average body weight of mice in each treatment groups during the study period. Tumor burden in lungs as quantified by **(E)** percentage of tumor lesion area per total lung area (see Supplementary Fig. S6A for images) and by **(F)** qPCR analysis of human *HPRT* (*hHPRT*) mRNA relative to mouse *HPRT* (*mHPRT*) in mouse lungs. **G**, Knockdown of *PLK1* mRNA, quantified by *hPLK1* mRNA expression in the lung tissues relative to *hHPRT* mRNA. *H*, human. **H**, Percentage of Ki-67-positive cells in the lung nodes (see Supplementary Fig. S6B for images). **F**, Percentage of cleaved caspase-3 (CC3)-positive cells in the lung nodes (see Supplementary Fig. S6C for images). All data are represented as average  $\pm$  SEM ( $n = 24$  for **(B)** and  $n = 8$ /group for **(C)** and **(D)**). Each dot in **(E-G)** represents value from one mouse and in **(H)** and **(I)** represents one tumor node in the lungs of mice ( $n = 2$  nodes/mouse, 5 mice/group). Data are presented as mean  $\pm$  SEM [ $n = 24$  for **(B)** and  $n = 8$ /group for **(C)** and **(D)**]. \*,  $P < 0.05$  from two-way ANOVA followed by Dunnett multiple comparison tests for **(C)** and **(D)**.  $P$  values as indicated on **(E-I)** from Kruskal-Wallis test.

immunofluorescent tissue images are shown in Supplementary Fig. S6. The data suggest a reduction in cancer metastatic potential to distant sites by the T-NP (with just siSCR), which is consistent with our *in vitro* data in Fig. 3, whereas siPLK1 on the nanoparticle inhibited cancer growth.

#### T-siPLK1-NP impedes tumor proliferation and promotes cancer apoptosis in the lungs

In addition to metastasis incidence rate and tumor burden, we carefully characterized the cancer in lungs of mice to confirm the treatment efficacy of T-siPLK1-NP. T-siPLK1-NP treatment significantly reduced the tumor lesion area (by H&E, which was confirmed by human vimentin staining) in lungs by 91% and 89% compared with the saline and T-siSCR-NP groups, respectively (Fig. 4E). The extent of human cancer in mouse lungs was also quantified by the relative levels of human *HPRT* (*hHPRT*) mRNA to mouse *HPRT* mRNA (*mHPRT*). In agreement with the histologic data, T-siPLK1-NP decreased *hHPRT* mRNA by 84% and 79% compared with the saline and T-siSCR-NP groups, respectively (Fig. 4F). Finally, we confirmed that the therapeutic

effect was the direct result of RNAi by assessing the level of *PLK1* knockdown. T-siPLK1-NP treatment effectively depleted *PLK1* gene expression by 84% and 81% compared with the saline and T-siSCR-NP groups, respectively (Fig. 4G). Immunostaining for Ki-67 and cleaved caspase-3 also confirmed that T-siPLK1-NP caused a significant reduction in overall proliferation (Fig. 4H) and an increase in apoptosis (Fig. 4I). Taken together, these experiments showed that our nanoparticle effectively delivered siPLK1 to metastatic tumors upon systemic delivery, which resulted in reduced tumor growth and increased cancer death.

#### Depletion of PLK1 by T-siPLK1-NP inhibits lung metastasis and prolongs overall survival in long-term *in vivo* study

To investigate the long-term therapeutic effect of T-siPLK1-NP treatment, we conducted a long-term study in which mice received the same dosing schedule as the short-term study but extended the study to 2 months (see dashed lines in Fig. 5A for injection days). Tumor burden was monitored up to day 32 after first treatment where more than 80% of mice were still alive. As expected,

Morry et al.

**Table 1.** Incidence rate of LM2-4luc<sup>+</sup>/H2N metastasis in various organs of mice receiving a total of 6 doses of either T-siPLK1-NP or T-siSCR-NP, as quantified by *ex vivo* IVIS imaging as shown in Supplementary Fig. S5C

Group	Parameter	Brain	Lung	Liver	Spleen	Kidney	Lymph nodes	Spine	Total tumor signal	Ratio over saline
Saline	Incidence rate	2/8	8/8	2/8	1/8	1/8	5/8	4/8	2,749	1.00
	Tumor signal	288	405	73	16	12	240	1,717		
T-siSCR-NP	Incidence rate	1/8	7/8	—	—	—	4/8	4/8	2,036	0.74
	Tumor signal	139	443	—	—	—	131	1,322		
T-siPLK1-NP	Incidence rate	—	4/8	—	—	—	1/8	3/8	968	0.35
	Tumor signal	—	26	—	—	—	3	939		

NOTE: The tumor signal in each organ is reported as fold change over the signal from the same organ of normal mice ( $n = 4$  for normal mice,  $n = 8$  mice per treatment group). Dose and schedule as shown in Fig. 4A.

T-siPLK1-NP significantly reduced tumor burden in the lungs as measured by 100-fold less of bioluminescence signal versus saline (Fig. 5A). Also, the T-siPLK1-NP treatment significantly prolonged the overall survival (Fig. 5B). In addition, upon sacrifice/death, we observed large axillary lymph node tumors ( $>1,200 \text{ mm}^3$ ) in multiple mice from the saline and T-siSCR-NP groups (4 of 8 in each group), whereas only 1 of 8 mice in the T-siPLK1-NP group exhibited large lymph node tumors. T-siPLK1-NP treatment also yielded smaller lung lesions as compared with saline and T-siSCR-NP groups (Supplementary Fig. S7), which agrees with the results from the short-term study. In summary, treatment with T-siPLK1-NP elicits antimetastatic activity and extends overall survival in mice, which provides a novel potential therapeutic option for metastatic breast cancer disease.

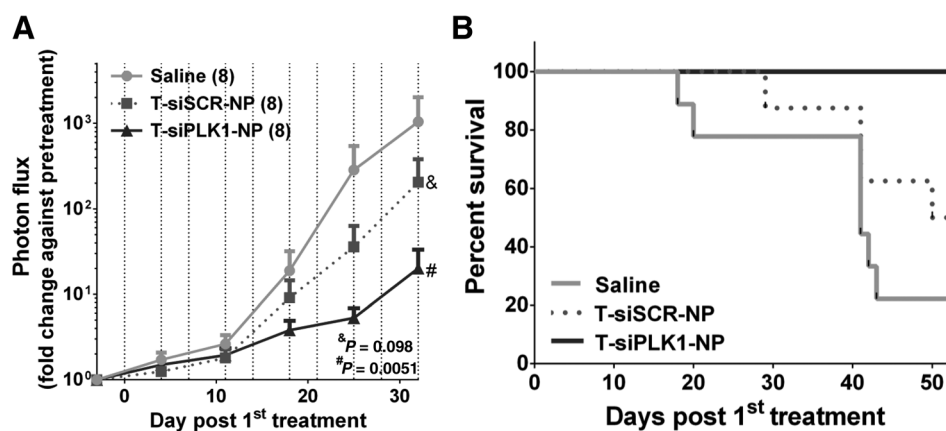
## Discussion

Herein, we have shown for the first time that MSNPs can scavenge intracellular ROS, modulate NOX4 activity, and in turn inhibit cellular invasion and migration in breast cancer cells *in vitro*. The ROS-scavenging ability of MSNP is thought to be contributed by its extremely large surface area with protonated sites (from the acid reflux to remove surfactants during the MSNP synthesis). This intrinsic property of MSNP further promotes its use as a therapeutic delivery platform for cancer treatment. We believe this finding is impactful, as it may inspire

new platforms that are not only passive carriers but also therapeutics. For human use, MSNP is more promising than other antioxidant nanoparticles (such as fullerene, platinum, cerium oxide) because MSNP is more benign and soluble at physiological pH to silicic acid for kidney clearance (30). Silicon (Si) is also the most abundant trace element in the human body after iron and zinc (31).

High-MW PEI ( $>20 \text{ kDa}$ ) is needed to form a dense siRNA-polyplex for good transfection efficacy (e.g., jetPEI, which underwent clinical trials (32)). We used smaller PEI (10 kDa) for less toxicity while enhancing efficacy by cross-linking the PEI layer. The cross-linking increased the buffering capacity (4) leading to greater endosomal escape of siRNA based on proton sponge effect principle (33). siRNA released from the PEI layer by displacement of heparan sulfate (similar size and charge with siRNA) and by reducing of the cross-linker by glutathione. The detailed mechanism will be reported in due course.

This nanotherapeutic (siRNA-nanoparticle) was effective in treating metastatic breast cancer by simultaneously reducing metastatic potential of cancer through the intrinsic antioxidant property of the nanoparticle and delivering siPLK1 to metastatic tumors to promote apoptosis in those tumors through *PLK1* gene silencing mechanism. As previously discussed, PLK1 inhibitors have shown to impart adverse effects, and siPLK1 on lipid nanoparticles without a targeting agent only provided a narrow therapeutic window in clinical trials. The sequence specificity of

**Figure 5.**

T-siPLK1-NP treatment improves overall survival of LM2-4luc<sup>+</sup>/H2N experimental metastasis mice. **A**, Quantification of lung photon flux normalized to pretreatment flux from each individual mouse in the treatment groups ( $n = 8/\text{group}$ ). Data are presented as mean  $\pm$  SEM.  $P$  values as indicated on the graph from two-way ANOVA followed by Dunnett multiple comparison tests. Vertical dashed lines represent injection days. **B**, Kaplan-Meier survival of mice ( $n = 8/\text{group}$ ). Data are presented as mean  $\pm$  SEM. \*,  $P = 0.0251$  between T-siPLK1-NP versus saline by Mantel-Cox log-rank test. H&E and DAPI/vimentin stains of lung samples can be found in Supplementary Fig. S7.

siPLK1 combined with the tumor-targeting ability of our nanoparticle platform will potentially improve both efficacy and safety for treating metastatic breast cancer. The unique antioxidant features and the versatility of our nanoparticles will potentially be beneficial in the treatment of not only cancer but also other fibrotic diseases.

### Disclosure of Potential Conflicts of Interest

OHSU, J. Morry, W. Ngamcherdtrakul, D.J. Castro, J.W. Gray, and W. Yantasee have a significant financial interest in PDX Pharmaceuticals, LLC, a company that may have a commercial interest in the results of this research and technology. This potential personal and institutional conflict of interest has been reviewed and managed by OHSU. No potential conflicts of interest were disclosed by the other authors.

### Authors' Contributions

**Conception and design:** J. Morry, W. Ngamcherdtrakul, J.W. Gray, W. Yantasee  
**Development of methodology:** J. Morry, W. Ngamcherdtrakul, S. Gu, W. Yantasee  
**Acquisition of data (provided animals, acquired and managed patients, provided facilities, etc.):** J. Morry, W. Ngamcherdtrakul, S. Gu, M. Reda, T. Sangvanich  
**Analysis and interpretation of data (e.g., statistical analysis, biostatistics, computational analysis):** J. Morry, S. Gu, J.W. Gray, W. Yantasee  
**Writing, review, and/or revision of the manuscript:** J. Morry, W. Ngamcherdtrakul, M. Reda, D.J. Castro, J.W. Gray, W. Yantasee

### References

1. Ferlay J, Soerjomataram I, Ervik M, Dikshit R, Eser S, Mathers C, et al. GLOBOCAN 2012 v1.1, cancer incidence and mortality worldwide: IARC CancerBase No. 11. Lyon, France: International Agency for Research on Cancer; 2014.
2. SEER Cancer Stat Facts: Female Breast Cancer. National Cancer Institute. Bethesda, MD. Available from: <http://seer.cancer.gov/statfacts/html/breast.html>.
3. Ngamcherdtrakul W, Castro DJ, Gu S, Morry J, Reda M, Gray JW, et al. Current development of targeted oligonucleotide-based cancer therapies: perspective on HER2-positive breast cancer treatment. *Cancer Treat Rev* 2016;45:19–29.
4. Ngamcherdtrakul W, Morry J, Gu S, Castro DJ, Goodyear SM, Sangvanich T, et al. Cationic polymer modified mesoporous silica nanoparticles for targeted siRNA delivery to HER2+ breast cancer. *Adv Funct Mater* 2015;25:2646–59.
5. Winkles JA, Alberts GF. Differential regulation of polo-like kinase 1, 2, 3, and 4 gene expression in mammalian cells and tissues. *Oncogene* 2005;24:260–6.
6. Degenhardt Y, Lampkin T. Targeting polo-like kinase in cancer therapy. *Clin Cancer Res* 2010;16:384–9.
7. Maire V, Nemati F, Richardson M, Vincent-Salomon A, Tesson B, Rigault G, et al. Polo-like kinase 1: a potential therapeutic option in combination with conventional chemotherapy for the management of patients with triple-negative breast cancer. *Cancer Res* 2013;73:813–23.
8. Hu K, Law JH, Fotovati A, Dunn SE. Small interfering RNA library screen identified polo-like kinase-1 (PLK1) as a potential therapeutic target for breast cancer that uniquely eliminates tumor-initiating cells. *Breast Cancer Res* 2012;14:R22.
9. Frost A, Mross K, Steinbild S, Hedbom S, Unger C, Kaiser R, et al. Phase I study of the Plk1 inhibitor BI 2536 administered intravenously on three consecutive days in advanced solid tumours. *Curr Oncol* 2012;19:e28–35.
10. Weiß L, Efferth T. Polo-like kinase 1 as target for cancer therapy. *Exp Hematol Oncol* 2012;1:38.
11. Raab M, Kappel S, Kramer A, Sanhaji M, Matthes Y, Kurunci-Csacsko E, et al. Toxicity modelling of Plk1-targeted therapies in genetically engineered mice and cultured primary mammalian cells. *Nat Commun* 2011; 2:395.
12. Arbutus. Arbutus Reports topline results from TKM-PLK1 HCC clinical trial. Vancouver, B.C. and Doylestown, PA: GLOBE NEWSWIRE; 2016.
13. Ramanathan RK, Hamburg SI, Borad MJ, Seetharam M, Kundranda MN, Lee P, et al. A phase I dose escalation study of TKM-080301, a RNAi

**Administrative, technical, or material support (i.e., reporting or organizing data, constructing databases):** W. Ngamcherdtrakul, W. Yantasee  
**Study supervision:** W. Yantasee

### Acknowledgments

The authors are grateful to Prof. Sara Courtneidge of OHSU for independent reviewing of the data in this article and to Prof. Robert Kerbel at the University of Toronto and Dr. Giulio Francia at the University of Texas at El Paso for the generous gift of LM2-4luc<sup>+</sup>/H2N breast cancer cell line. We thank Dr. Shinji Iizuka for sharing his expertise on the gel degradation/invasion assays. We thank Tiera Liby in Gray's laboratory for TNBC cell lines. We also thank the Transgenic Core of Oregon Health and Science University (Dr. Lev Fedorov) for SCID hairless SHO mouse breeding.

### Grant Support

This work was funded by NIH/NCI contract #HHSN261201300078C (W. Yantasee, W. Ngamcherdtrakul, D.J. Castro, J.W. Gray), the Prospect Creek Foundation (J.W. Gray, W. Yantasee), and OHSU's VPR fund (W. Yantasee).

The costs of publication of this article were defrayed in part by the payment of page charges. This article must therefore be hereby marked *advertisement* in accordance with 18 U.S.C. Section 1734 solely to indicate this fact.

Received September 29, 2016; revised December 13, 2016; accepted December 18, 2016; published OnlineFirst January 30, 2017.

- therapeutic directed against PLK1, in patients with advanced solid tumors. *Cancer Res* 2013;73(8 Suppl): Abstract nr LB-289.
14. Liou GY, Storz P. Reactive oxygen species in cancer. *Free Radic Res* 2010;44:479–96.
  15. Diaz B, Shani G, Pass I, Anderson D, Quintavalle M, Courtneidge SA. Tks5-dependent, nox-mediated generation of reactive oxygen species is necessary for invadopodia formation. *Sci Signal* 2009;2:ra53.
  16. Boudreau HE, Casterline BW, Rada B, Korzeniowska A, Leto TL. Nox4 involvement in TGF-beta and SMAD3-driven induction of the epithelial-to-mesenchymal transition and migration of breast epithelial cells. *Free Radic Biol Med* 2012;53:1489–99.
  17. Zhang C, Lan T, Hou J, Li J, Fang R, Yang Z, et al. NOX4 promotes non-small cell lung cancer cell proliferation and metastasis through positive feedback regulation of PI3K/Akt signaling. *Oncotarget* 2014;5: 4392–405.
  18. Hong SY, Gil HW, Yang JO, Lee EY, Kim HK, Kim SH, et al. Effect of high-dose intravenous N-acetylcysteine on the concentration of plasma sulfur-containing amino acids. *Korean J Intern Med* 2005;20: 217–23.
  19. Cifuentes-Pagano E, Meijles DN, Pagano PJ. The quest for selective nox inhibitors and therapeutics: challenges, triumphs and pitfalls. *Antioxid Redox Signal* 2014;20:2741–54.
  20. MBCAlliance. Metastatic breast cancer landscape analysis: research report October 2014. New York, NY: Metastatic Breast Cancer Alliance; 2014.
  21. Clogston JD, Patri AK. NCL method PCC-2: measuring zeta potential of nanoparticles. Frederick, MD: Nanotechnology Characterization Laboratory; 2009.
  22. Francia G, Man S, Lee CJ, Lee CR, Xu P, Mossoba ME, et al. Comparative impact of trastuzumab and cyclophosphamide on HER-2-positive human breast cancer xenografts. *Clin Cancer Res* 2009;15:6358–66.
  23. Morry J, Ngamcherdtrakul W, Gu S, Goodyear SM, Castro DJ, Reda MM, et al. Dermal delivery of HSP47 siRNA with NOX4-modulating mesoporous silica-based nanoparticles for treating fibrosis. *Biomaterials* 2015;66: 41–52.
  24. Wang Z, Li Y, Sarkar FH. Signaling mechanism(s) of reactive oxygen species in epithelial-mesenchymal transition reminiscent of cancer stem cells in tumor progression. *Curr Stem Cell Res Ther* 2010;5:74–80.
  25. Liang CC, Park AY, Guan JL. *In vitro* scratch assay: a convenient and inexpensive method for analysis of cell migration *in vitro*. *Nat Protoc* 2007;2:329–33.

Morry et al.

26. Le Gal K, Ibrahim MX, Wiel C, Sayin VI, Akula MK, Karlsson C, et al. Antioxidants can increase melanoma metastasis in mice. *Sci Transl Med* 2015;7:308re8.
27. Kenny PA, Lee GY, Myers CA, Neve RM, Semeiks JR, Spellman PT, et al. The morphologies of breast cancer cell lines in three-dimensional assays correlate with their profiles of gene expression. *Mol Oncol* 2007;1:84–96.
28. Munoz R, Man S, Shaked Y, Lee CR, Wong J, Francia G, et al. Highly efficacious nontoxic preclinical treatment for advanced metastatic breast cancer using combination oral UFT-cyclophosphamide metronomic chemotherapy. *Cancer Res* 2006;66:3386–91.
29. Milsom CC, Lee CR, Hackl C, Man S, Kerbel RS. Differential post-surgical metastasis and survival in SCID, NOD-SCID and NOD-SCID-IL-2R $\gamma$ (null) mice with parental and subline variants of human breast cancer: implications for host defense mechanisms regulating metastasis. *PLoS One* 2013;8:e71270.
30. Tam D, Ashley CE, Xue M, Carnes EC, Zink JI, Brinker CJ. Mesoporous silica nanoparticle nanocarriers: biofunctionality and biocompatibility. *Acc Chem Res* 2013;46:792–801.
31. Jugdaohsingh R. Silicon and bone health. *J Nutr Health Aging* 2007; 11:99–110.
32. Sidi AA, Ohana P, Benjamin S, Shalev M, Ransom JH, Lamm D, et al. Phase I/II marker lesion study of intravesical BC-819 DNA plasmid in H19 over expressing superficial bladder cancer refractory to bacillus calmette-guerin. *J Urol* 2008;180:2379–83.
33. Behr JP. The proton sponge: a trick to enter cells the viruses did not exploit. *CHIMIA Int J Chem* 1997;51:34–6.

# Molecular Cancer Therapeutics

## Targeted Treatment of Metastatic Breast Cancer by PLK1 siRNA Delivered by an Antioxidant Nanoparticle Platform

Jingga Morry, Worapol Ngamcherdtrakul, Shenda Gu, et al.

*Mol Cancer Ther* 2017;16:763-772. Published OnlineFirst January 30, 2017.

**Updated version** Access the most recent version of this article at:  
doi:[10.1158/1535-7163.MCT-16-0644](https://doi.org/10.1158/1535-7163.MCT-16-0644)

**Supplementary Material** Access the most recent supplemental material at:  
<http://mct.aacrjournals.org/content/suppl/2017/01/28/1535-7163.MCT-16-0644.DC1>

**Cited articles** This article cites 27 articles, 6 of which you can access for free at:  
<http://mct.aacrjournals.org/content/16/4/763.full#ref-list-1>

**E-mail alerts** [Sign up to receive free email-alerts](#) related to this article or journal.

**Reprints and Subscriptions** To order reprints of this article or to subscribe to the journal, contact the AACR Publications Department at [pubs@aacr.org](mailto:pubs@aacr.org).

**Permissions** To request permission to re-use all or part of this article, contact the AACR Publications Department at [permissions@aacr.org](mailto:permissions@aacr.org).